Research Square

Preprints are preliminary reports that have not undergone peer review.
They should not be considered conclusive, used to inform clinical practice,
or referenced by the media as validated information.

Tumor-mediated shape-transformable nanogels with pH/redox/enzymatic-sensitivity for anticancer therapy

Dong Zhou
Hubei University
Sainan Liu
Hubei University
Yongjun Hu
Hubei University of Chinese Medicine
Shiwei Yang
Hubei University
Bing Zhao
Hubei University
Kaikai Zheng
Hubei University
Yuhong Zhang
Hubei University
Peixin He
Hubei University
Guoyan Mo
Hubei University of Chinese Medicine
Yulin Li (yulinli@uma.pt)
East China University of Science and Technology

Research

Keywords: Biodegradable nanogels, Tumor-mediated shape transformability, pH/redox/enzymatic-stimulative, Doxorubicin, Selective drug delivery

Posted Date: December 16th, 2019

DOI: https://doi.org/10.21203/rs.2.18852/v1

License: This work is licensed under a Creative Commons Attribution 4.0 International License.
Read Full License

Abstract

Background

Delivery of anticancer drug(s) throughout tumor tissues is critical for cancer therapy. However, most current nanomedicines lack sufficient tumor permeability due to their bulky size (100 ~ 200 nm), which is a main reason for clinical failure in tumor chemotherapy up to now.

Results

To overcome this challenge, we developed a kind of tumor-mediated transformable chitosan-based nanocarriers with surface-charge adjustability via self-assembly and double-crosslinking approach. Their surface-charge variation allowed for selective administration of drugs of specific charges. The nanomedicine maintained good colloidal stability, and upon arrival under the reducible and lysozyme-expressed microenvironments mimicking tumor tissues, one nanomedicine was cleaved to release around one thousand ultrasmall nanovesicles (4 ± 1 nm). This size transformability allowed for their passing through the depth of solid tumor tissues to achieve an effective therapeutic delivery into cancer cells to enhance antitumor efficacy, suggesting its potential use as a platform for therapeutic delivery.

Conclusions

Our work provide a strategy to develop tumor-stimulative shape-transformable nanoplatform for anticancer drug delivery.

Background

Nanotechnologies continue to prompt the fast development of new methodologies for the creation of drug delivery nanosystems. Several anticancer nanomedicines have been clinically developed thus far, and others are currently being investigated at a clinical trial stage[1]. Although numerous nanocarriers have been proven to be effective in animal models, most fail to pass clinical trials due to poor antitumor efficacy and high toxicity. In the context of standard cancer treatment via intravenous administration of drug to the patient, nanomedicines must overcome numerous biological barriers (i.e., circulation, accumulation, penetration, internalization, and release)[2]. Therefore, an ideal delivery system must not only carry drugs with cancer selectivity, but also own combinative delivery merits, including (1) relatively high colloidal stability to offer long-term circulation in the blood vessels[3-5], (2) sufficient accumulation in the tumor[6], (3) ability to pass through avascular tumor tissue[7], (4) easy uptake by cancer cells for efficient internalization[8, 9], (5) effective intracellular drug release[10, 11]. Facing the high requirements, the lack of drug loading selectivity, and the passiveness in delivery of the payloads into tumor tissue and to distal tumor cells from blood vessels remain the main unresolved obstacles. For instance, liposomal-based Doxil nanomedicine (a type of FDA-approved anticancer nanomedicine carrying doxorubicin (DOX))[12], which accumulates around solid tumors in a better way than free DOX, is severely restricted within the perivascular regions on extravasation. The self-assembled liposomal structure may be

unstable in system circulation, resulting in drug leakage in healthy tissues[13]. The large size of bulky nanomedicines and the passive nature of drug release limit their ability to pass through a compact paracellular matrix against the interstitial fluid pressure gradient[14, 15]. These shortcomings may be important reasons for the clinical failure of such nanomedicines, as well as for their severe side effects and poor therapeutic efficacy.

Nanomedicines with controllable architecture and properties create particular interactions with biological systems, which can be used for controlled delivery of therapeutic agents from the injection site to biological targets according to different stimuli[16, 17]. Several reports have demonstrated that the physicochemical properties of nanoparticles (such as size, shape, surface charge, and deformability) determine their interaction with biological systems during transportation[18-20]. The rapid cell-responsiveness of nanogels, which mimic soft tissue, raises the hypothesis that the hydrophilic nature of soft nanoparticles may lead to long-lasting colloidal stability during blood circulation[21], minimizing the possibility of entrapment by macrophages[22]. More importantly, certain crosslinks that are cleavable by the tumor-specific pathological signal(s) can be introduced into nanogels to offer stimulation-triggered therapeutic release and stepwise-degradable nanoblocks of smaller size. The stepwise-biodegradability, combined with their enhanced deformability, endows them with high tissue-penetration capacity and enables the penetration in solid tumors[23]. Furthermore, nanogels can be more efficiently taken up by cells than conventional nanocarriers (e.g., liposomes)[24], resulting in improved bioavailability and safety profile *in vivo*[25]. Moreover, nanogels could be designed with specific properties required for the administration of drugs in a selective manner[26].

It is known that pH value differs between normal tissue (pH 7.4) and tumor extracellular microenvironment (pH ~ 6.8)[27-30]. Tumor tissues are characterized by an increased reductive potential, owned to the fact that tumor cells overexpress glutathione (GSH). The intracellular compartments of the tumors present acidic conditions (pH 4.0-6.0) and over-reductive state (1-10 mM, ~ 1000 times higher than that of extracellular ones)[31, 32]. Recent studies indicated that several tumor tissues also overexpressed lysozyme by 70-100 folds compared to normal tissues[33, 34]. The differences in endogenous signaling pathways of tumor tissue/cells could be exploited in efforts to develop tumor-triggered drug delivery nanosystems.

Herein, we aimed at designing a delivery system, which maintains colloidal stability (via double-crosslinking) in blood circulation, while having increased tumor penetration and cellular uptake ability through the tumor-mediated release of smaller nanoblocks, as well as enhanced intracellular accumulation of the drug through delivery triggered by endogenous tumor-specific signals. Based on these design properties, we proposed an approach to develop a tumor-induced cleavable nanogels with controlled surface charge. Negatively charged nanogels could be used for delivery of cationic anticancer drugs (e.g., doxorubicin), while positively charged for administering negatively charged nucleic acids (e.g., plasmid DNA). The nanogels with controlled surface-charge are synthesized via a double-crosslinking technique in combination with self-assembly of an anionic oligomer. During this process, native nanogels are fabricated through a quick gelation initiated by dual crosslinking of chitosan (bioactive natural

polymer with antitumor, immunostimulatory, antioxidant, antimicrobial activities)[35, 36] with sodium tripolyphosphate (ionic crosslinker) and N, N'-bisacrylamide cystamine (chemical crosslinker to offer redox cleavability). The double crosslinked nanogels are then submerged into a solution of poly(acrylic acid) oligomer to acquire negative-charged nanocarriers.. The resulting nanomedicine can be cleavable in the reductive and lysozyme-high tumor microenvironment. The tumor-mediated cleavability of the nanogels results in the release smaller nanoblocks carrying payloads that can penetrate the tumor[37-39]. The combined benefits of the nanocarriers result in a profoundly improved antitumor efficacy *in vivo* than free DOX drug. In fact, mice treated with the drug-loaded nanogels showed prolonged survival compared to free DOX-treated mice. The excellent biocompatibility and high antitumor bioactivity make nanocarriers very promising nanoplatforms for antitumor drug delivery.

Experimental Section

Materials

Chitosan (CTS) and dithiothreitol (DTT) were obtained from Sinopharm Chemical Reagent Co., Ltd, China. Carboxymethyl chitosan (CMCC) was purchased from Hefei Bomei Biotechnology Co., Ltd, China. Sodium tripolyphosphate (TPP) and polyacrylic acid (PAA with an average molecular weight of 3,000 Da) were obtained from Aladdin Chemical Reagent Co., Ltd, China. N, N'-bisacrylamide cystamine (BAC) was purchased from Alfa Aesar A Johnson Matthey Company, China. Doxorubicin hydrochloride (DOX) was obtained from Dalian Meilun Biotechnology Co., Ltd, China.

Preparation of nanogels

1% acetic acid was used to dissolve CTS to obtain a 1 mg/mL CTS solution (pH 5.5), followed by the addition of TPP and CMCC solutions. BAC solution was then introduced into the above system. After reaction for 12 h, the mixture was purified using a dialysis bag (MWCO: 8,000 - 1,4000 Da) to obtain CTCB nanogels. For surface modification, the CTCB nanogels were mixed with different concentrations of PAA and then underwent dialysis.

Drug loading and release study

Positively charged CTCB nanogels were tested for loading of negatively-charged red fluorescent plasmid DNA (Marker IV) constructed from Marker D2000 as described previously[40]. The DNA solution (350 μg/mL) was mixed with CTCB solution (8 mg/mL). After centrifugation at 15,000 × *g* for 30 min, the precipitate and the supernatant underwent gel electrophoresis analysis**.** For cationic drug delivery, 1 mL of DOX solution (1 mg/mL) was mixed with 5 mL of aqueous solution (8 mg/mL) of nanogels (CTCB and CTCP). After overnight magnetic stirring, the mixtures were purified using a dialysis membrane (MWCO: 8,000 - 14,000 Da) to offer DOX@CTCB and DOX@CTCP, respectively. The dialysate was collected, and its absorbance at 490 nm was measured using a UV spectrophotometer (UV-6100S). For drug release studies, 1 mL of dialysis sample was added in 30 mL of PBS solution with different pH values (5.0, 6.5, 7.4), in the absence or presence of dithiothreitol (DTT; 5 mM or 10 mM) and/or lysozymes (0.5 mg/mL or

1 mg/mL). At different time points, the amount of released drug was determined via UV analysis. Percentage of DOX released from nanocarriers was determined according to the equation:

$$C_r = 100 * W_t / W_{tot} \quad (1)$$

where W_t is the cumulative amount of drug released at time t, and W_{tot} is the total drug amount contained in the nanogels.

Characterization of nanogels

The microstructure of samples was investigated on a Fourier Transform Infrared (FTIR) spectrometer (Perkin-Elmer, USA) and Rama spectrometer (Renishaw, France). Transmission electron microscope (TEM, Tecnai G20, USA) was used to assess the morphology and size of the nanoparticles. Briefly, a drop of the sample (0.5 mg/mL) was loaded onto a copper mesh of carbon support film and placed in a fume hood to air-dry overnight. The colloidal stability of the nanogel solution was determined using an optical digital camera. The hydrodynamic diameter and surface charges of the nanogels in water or PBS were measured using a Zetasizer (Nano ZS, Malvern Instruments).

Cell culture and viability assay

A549 cells (human lung adenocarcinoma cell line) and cell counting kit-8 (CCK-8) were used to assess the cytotoxicity of drug-loaded nanoparticles. When A549 cell confluence reached 80%, cells were detached using 0.25% trypsin containing EDTA and seeded into 96-well plates at 5×10^5 cells/well. After 24 h incubation, fresh DMEM (200 μL) medium containing DOX, DOX@CTCB, or DOX@CTCP in equivalent concentrations (0.5 μM, 1 μM, 2 μM, 2.5 μM, 3 μM) was added into each well. Cells treated with DMEM alone and CTCB or CTCP served as a negative control. Cell viability was assessed via CCK-8 assay after 48 h of treatment. OD absorbance was measure at 450 nm, and cell viability was determined using the following equation:

$$Cell\ \ Viability\ (\%) = OD_{eg} / OD_{cg} \times 100\ \% \quad (2)$$

where OD_{eg} and OD_{cg} are the OD values for the experimental group and control group, respectively.

Cell uptake assay

A549 cells were seeded into 20 mm culture dishes at a density of 1×10^6 cells per dish and incubated at 37 °C and 5% CO_2. After 24 h of incubation, DOX, DOX@CTCB, DOX@CTCP nanogels with equivalent DOX concentration (2 μM) were added, followed by incubation for 4 h and 24 h. The drug-containing cell medium was removed, and cells were washed with PBS (pH 7.4) three times. Cells were then fixed with 4% paraformaldehyde for 30 min. After washing with PBS (pH 7.4), cell nuclei were stained with Hoechst 33342 in the dark. The dishes were observed by Confocal Laser Scanning Microscope (CLSM, Nikon C2, Japan).

Hemolysis assay

The hemolytic properties of nanoparticles were tested using rat blood, as described previously[41]. Briefly, 2 mL of 2% red blood cell (RBC) suspensions were exposed to the equivalent volume of nanogel solution (to ensure that the final nanogel concentration ranged from 0.19 mg/mL to 3.00 mg/mL). RBC incubation with sterile D.I. water and saline injection solution were used as positive and negative controls, respectively. After 3 h incubation at 37 °C, suspensions were centrifuged at 12,000 × *g* for 10 min. The supernatant of each sample was transferred in 96-well culture plate in triplicate to measure the absorbance of the released hemoglobin. Absorbance at 570 nm was measured using a SpectraMax iD3 multi-function reader (Molecular Devices Company, USA). The hemolysis ratio was calculated using the following formula (3):

$$Hemolysis\ \ Rate\ (\%) = (A_S - A_N) \ / \ (A_P - A_N) \times 100 \qquad (3)$$

where A_S, A_N, and A_P represent the average absorbance of the samples, negative controls, and positive controls, respectively.

In vivo antitumor studies

All experiment protocols were approved by the Institutional Animal Care and Use Committee (IACUC) of the Animal Experiment Center of Wuhan University of Chinese Medicine (Wuhan, China). C57BL/6J mice were purchased from the Hubei Experimental Animal Research Center. H22 liver tumor-bearing mice (tumor size: 200 mm^3) were randomly divided into three groups (five mice per group). The mice were intraperitoneally injected with PBS, DOX, DOX@CTCP, twice per day for a total of 6 doses. The dose of DOX was 4 mg/kg per mouse. Tumor size and mouse weight were recorded before injection. The tumor volume was determined as follows: V = ((tumor length) × (tumor width)^2)/2. V/V_0 *and* M/M_0 represent the relative tumor volume ratio and the relative body weight ratio, respectively. V_0 and M_0 were the tumor volume and body weight before the treatment, respectively.

In vivo biocompatibility/biosafety

In order to evaluate the systemic toxicity, mice were culled after treatment. The major organs, including spleen, kidney, heart, liver, and tumors, were collected and subjected to hematoxylin-eosin (H&E) staining to evaluate histological characteristics.

Results And Discussion

Preparation of size and surface-charge controllable nanogels

To overcome the passive nature of drug delivery using traditional liposomal nanocarriers with unstable micelle structure[42], we aimed at developing a novel type of double-crosslinked nanogels to achieve the administration of therapeutic agents in a selective active way. The Food and Drug Administration (FDA)-approved natural-derived polymer[43], chitosan with lysozyme-cleavability, was selected as a model matrix for modification of the biodegradable nanogels. Chitosan was transformed into single-crosslinked nanogels through its ionic crosslinking with sodium tripolyphosphate (TPP; used as a pH mediator) in the

presence of carboxymethyl chitosan (CMCC), which is more hydrophilic than CTS, improving the colloidal stability of the latter[44]. In order to further improve their structural stability and delivery sensitivity, N, N'-bisacrylamide cystamine (BAC) was introduced, resulting in positively-charged nanogels (CTCB) with a secondary redox-sensitive crosslink. After that, an oligomer of poly(acrylic acid) (PAA) rich in –COOH groups and with an ability to prevent aggregation of nanoparticles[45], was selected for decoration of the nanogels (Figure S1) and adjustment of the surface-charge (from positive into a negative state). The resulting negatively-charged nanogels (CTCP) were used for loading the cationic anticancer drug doxorubicin (DOX). The formation of DOX@CTCP is driven by the formation of hydrogen bonds in DOX, CMCC, and CTS. PAA chains bind the $–NH_2$ of CTS via electrostatic interactions. Additionally, the chelation between DOX and PAA, as well as the hydrogen bonds between DOX and PAA, enabled an efficient encapsulation of DOX into CTCP.

After optimization, this technology allowed for the development of spherical CTCB and CTCP nanogels with hydrodynamic sizes of 191 ± 5 nm and 96 ± 2 nm, respectively. These sizes, which are similar to the clinically-used nanomedicines (100 ~ 200 nm), are appropriate for administration via intravenous injection,.CTCP nanogels were determined by TEM to have a size of ~ 50 nm (similar to that of CTCB nanogels; Figure S4), which can be cleaved to release nanoblocks of smaller sizes (4 ± 1 nm) (Figure 1B and Figure S2). The hydrodynamic diameter of the nanogels can be easily modified by variation of the compositional formulations (i.e., TPP/CTS feed ratio) (Figure 1C and Figure S3). For instance, nanogel sizes can be adjusted from 186 ± 3 nm to 361 ± 3 nm by increasing CTS concentration from 0.10 mg/mL to 1.25 mg/mL. Furthermore, the nanogel surface charge can be finely adjusted via conjugation with anionic PAA oligomers of different concentrations. In the absence of PAA, the chitosan-based nanogels (CTCB) had a positively-charged surface, while conjugation with 8 mg/mL PAA transformed the surface charge from 39.2 ± 7.1 mV into -26.8 ± 2.1 mV (Figure 1D). The nanogels were subjected to Fourier-transform infrared (FTIR) spectroscopy for microstructural investigation. As shown in Figure 1E, the native peaks of chitosan at 1599 cm^{-1} and 1083 cm^{-1} disappeared in the CTCB nanogels, suggesting that electrostatic interactions occurred between the amino groups in chitosan and the phosphate groups of TPP[46]. The peaks at 1700 cm^{-1} and 890 cm^{-1} may have resulted from carboxymethyl-chitosan, which participated in the formation of the nanogels[47, 48]. From Rama spectra analysis, a new peak at 513 cm^{-1} (corresponding to the absorbance of disulfide bonds) appeared in the nanogels[49], indicating that the redox-crosslinks were successfully introduced in the nanogels probably via Michael addition between the double bonds of BAC and the amino groups of chitosan[50,51]. As such, nanogels with controllable size and adjustable surface-charge have been successfully developed. The surface charge adjustability of the nanogels may be useful for the administration of specific drugs which have unique anionic or cationic charges.

Selective drug-loading capacity of the nanogels and their multi-stimulative drug release performance in tumor-mimicking microenvironments

As mentioned above, the physical properties of nanocarriers play an important role in drug delivery property. It is proposed that positively-charged nanoparticles are appropriate for encapsulation of negatively-charged therapeutic agents[52], while negatively-charged ones can be used for the loading of cationic drugs[53]. To verify our hypothesis, test drugs with reverse charges (plasmid DNA as a negatively-charged drug, and doxorubicin as a cationic drug) were selected for assessing the delivery selectivity of the developed nanocarriers. The electrophoretic analysis indicated that the positively-charged CTCB nanogels were able to encapsulate pDNA, probably through the formation of electrostatic interactions (Figure 2A).

Moreover, the negatively-charged CTCP nanogels obtained after PAA-conjugation enabled the effective loading of the cationic drug DOX. CTCP nanogels presented a high DOX encapsulation efficiency (EE: 92.1 ± 3.6%), which was approximately seven times higher than that of the cationic CTCB nanogels (EE: 13.4 ± 6.2%). Therefore, the nanogels developed with our approach presented a selectivity in the administration of oppositely-charged drugs, suggesting them to be an improved nanoplatform that can be used for selective delivery of drugs in a variety of biomedical applications.

The amount of drug(s) released from the nanocarriers is of high importance in execution of therapeutic bioactivity[54, 55]. Considering the complexity of the multiple barriers in tumor tissues, it is challenging to develop “smart” delivery systems able to sense the differences between normal conditions and the pathological tumor tissues. The pH, redox balance, and enzymatic properties have emerged as the most promising approaches for tumor selectivity[56]. DOX can be released continuously from the nanogels, reducing the possibility of toxic burst-release of free DOX and maintaining a long-term anticancer activity. Compared to the physiological environment (pH 7.4), the DOX was more easily released under acidic conditions representing the environment of solid tumors (pH 6.5) and endo/lysosomes (pH 5.0). This means that the majority of DOX can selectively be released from the nanogel under acidic conditions, increasing its selectivity to tumor tissues[57].

It was reported that GSH concentration in tumors is profoundly higher than in healthy tissues[58]. Additionally, the concentration of GSH in intracellular compartments is approximately 1,000 times higher than in normal extracellular conditions[59]. Therefore, tumors have an increased reductive potential compared to healthy tissues. To test the redox-sensitivity of the nanogels, the drug release profiles of the nanogels were assessed under tumor-mimicking microenvironments. Compared to physiological conditions, the nanogels showed an increased release rate and efficiency of DOX under a reducing environment. The release profile of redox-sensitive drugs may be related to the cleavage of the disulfide-crosslinks at high GSH concentrations, accelerating drug release and release efficiency[60]. Furthermore, nanogels have enzymatic sensitivity to lysozyme, a type of endogenous enzyme overexpressed in tumor tissues. Indeed, it was found that the presence of 0.5 mg/mL lysozyme resulted in almost a 2-fold increase in DOX release compared to the nanogels in the absence of lysozyme[61]. Treatment with lysozyme at 1.0 mg/mL resulted in a nearly complete release of DOX after 48 h, indicating that all the payload can be released from the nanocarriers to exert its antitumor activity. The drug release acceleration may be a consequence of their lysozyme-induced degradability, which can, in theory, result in

the release of approximately one thousand smaller-sized nanoblocks (4 ± 1 nm) carrying the loaded drug from the cleavage of a single nanogel (Figure 1). The pH/redox/enzymatic- sensitivity of the nanogels is intriguing and promising to achieve multi-factor-mediated selective drug release upon arrival at the tumor environment and intracellular compartments, enhancing antitumor efficacy and minimizing side effects[62].

In vitro cyto-biocompatibility and growth inhibition in cancer cells

The main obstacles for anticancer drug delivery lie in the toxicity of the nanocarriers themselves, as well as the lack of controlled drug delivery at the right time and place[63]. Therefore, it is essential to develop novel biocompatible nanocarriers. We first sought to ascertain the cyto-biocompatibility of the nanogels. The hemolysis assessed by ASTM F756-00 indicated that both CTCB and CTCP nanogels are hemolytic (Figure 3D and Figure S6)[64]. Meanwhile, A549 cells maintained > 95% cell viability after their incubation with CTCP nanogels at concentrations up to 27.8 μg/mL, suggesting that they belong to first-grade biocompatible materials and are safe to be used in biomedical applications.

Before studying the therapeutic efficacy of DOX@CTCP nanogels *in vivo*, we tested their therapeutic toxicity against cancer cells using the cell counting kit-8 (CCK-8) assay. Human lung adenocarcinoma cells (A549) were incubated with free DOX and DOX@CTCP at different DOX concentrations for 48 h. DOX@CTCP exhibited higher toxicity against cancer cells than free DOX or DOX@CTCP of the same dose (Figure 3A and Figure S5). DOX@CTCP had an IC50 of 0.73 μM, which was 2.6 times less than that of free DOX (1.89 μM). The more potent cancer cell growth-inhibitory capacity of DOX@CTCP may be associated with their high DOX-loading capacity and multi-factor-mediated drug release properties, leading to an enhanced cell uptake and consequent increased intracellular accumulation of DOX (Figure 3E and 3F, Figure S7). A549 cells cultured with free DOX maintained their physiological fusiform shape, which may be related to the multidrug resistance (MDR) of these tumor cells[65]. However, A549 cells exposed to DOX@CTCP lost their spindle-like morphology, indicative of cell apoptosis, and suggesting that the efficient intracellular delivery of DOX may overcome the MDR. Therefore, the selective DOX administration using CTCP nanogels allows for the effective delivery of DOX into cancer cells to exert potentiated antitumor activity.

DOX@CTCP nanogels show enhanced antitumor activity in tumor-bearing mice

Due to the improved anti-proliferative effects of DOX@CTCP nanogels in cancer cells in vitro, we sought to investigate their antitumor potential *in vivo*. C57BL/6J male mice bearing H22 hepatocarcinoma tumors were randomly allocated into three groups (n = 5 per group) and received the following treatments: free DOX, saline, or DOX@CTCP. The doses of free DOX and DOX@CTCP were 4 mg/kg for each mouse. Tumor volume and body weight were monitored throughout the treatment period (7 d for free DOX control due to the earlier death of these mice, 15 d for saline control, and DOX@CTCP group). As shown in Figure 4A, in the course of the treatment, the tumor volume of mice treated with saline continued to increase. The administration of free DOX partially inhibited tumor growth, due to the cytotoxic activity of DOX mainly through disrupting the native double helix structure of DNA[66].

Treatment with DOX@CTCP showed the strongest inhibitory effect on tumor growth, presumably due to their pH/redox/enzymatic-mediated drug delivery properties, which render them with the ability to overcome tumor barriers and to enhance the intracellular drug accumulation in tumor cells (Figure 3 and Figure 4A). Images of the resected tumors (Figure 4B) again indicated that mice treated with DOX@CTCP had tumors of a profoundly smaller size.

Moreover, mice treated with free DOX experienced a rapid decrease in their body weight (Figure 4C), possibly due to the systemic toxicity of free DOX on the mice with higher tumor burden. Interestingly, the body weight of the mice treated with the DOX@CTCP group gradually increased during the treatment period, similar to those treated with saline group, indicating the good biocompatibility and low systemic toxicity of the nanogels. All the mice treated with free DOX group died until day 7, while the mice from the DOX@CTCP group survived throughout the chemotherapeutic period (15 d).

After mice were sacrificed, the tumor was excised and sectioned, followed by H&E staining. The microscopy (Figure 4D) indicated that significant tumor apoptosis/necrosis occurred in the tumors of mice treated with DOX@CTCP, while tumors from the mice treated with free DOX or saline had profoundly less necrotic areas. The biocompatibility and biosafety of the DOX@CTCP nanoplatform were further evaluated by histological assay. H&E staining images in sections from vital organs (heart, liver, spleen, and kidney) suggested severe damage when mice were treated with free DOX. However, no apparent pathological tissue damage appeared in organs of mice treated with DOX@CTCP, suggesting negligible side effects in non-malignant tissues.

Several inorganic nanoparticles and their nanohybrids with organic systems have been tested for the delivery of DOX. These studies have shown that the inorganic compositions can increase the drug encapsulation efficiency[67, 68]. However, the previously reported platforms lack sufficient biodegradability, resulting in limited release efficiency and non-controlled delivery[69]. Here, the natural polymer chitosan was used as a matrix for the development of degradable nanogels, which can minimize the potential risks of inorganic materials (e.g., long-term accumulation side effects) in the body[70]. The surface adjustment strategy employed in this study could be applied for the delivery of other drugs or proteins (such as DNA, RNA, and enzymes). The nanosystems described here offer a high drug encapsulation efficiency (92.1%), which is significantly higher than that of previous DOX carriers (~ 4%) [71]. More importantly, nearly 100% of the loaded drug was released in tumor mimicking microenvironments, resulting in a 2.6-fold decrease in IC50 compared to free DOX. Most previous DOX-loaded inorganic systems (e.g., mesoporous silica (MSN), carbon nanotube (CNT), and hydroxyapatite (HAp)) showed higher IC50 than free DOX probably due to a limited release efficiency[72]. These characteristics, along with the multi-factor-induced drug release, endow the DOX@CTCP nanogels with great potential as an antitumor chemotherapeutic agent, while having minimal toxic side effects.

Conclusions

In summary, we reported a multifunctional nanoplatform, allowing for a highly effective antitumor activity through the selective administration of the therapeutic agent. This is achieved by the synthesis of a kind of positively-charged tumor-mediated cleavable nanogels via the double-crosslinking of chitosan with sodium tripolyphosphate and disulfide-containing molecule. After assembly with an oligomer of poly(acrylic acid), the cationic nanogels are transformed into negatively-charged ones (CTCP). Positively-charged nanogels can be used for administration of anionic drug(s) (e.g., plasmid DNA), while negatively-charged nanogels can deliver cationic drug(s) (e.g., doxorubicin, DOX). The developed DOX-loaded CTCP is cleavable under the GSH- and lysozyme-high, reductive tumor microenvironment to release smaller-sized nanoblocks. The unique features of this platform enable the multi-factor-mediated delivery of anticancer drugs in the acidic, reductive, and lysozyme-overexpressed tumor microenvironments, achieving an enhanced antitumor efficacy and improved biocompatibility than the free drug. Moreover, the transformable nanogels developed by our approach may be extended to administer the other types of chemotherapeutic agents (for co-delivery therapy via administration of DNA, siRNA, and other small molecular drugs) of interests, as a general novel nanoplatform with specific functions for disease treatment.

Declarations

Acknowledgments

This research was supported by the National Natural Science Foundation of China (81772317, 51973060). The funding from the CHUTIAN Scholar Project of Hubei Province and the Key Laboratory for the Synthesis and Application of Organic Functional Molecules, Ministry of Education (2014-KL-004) were also acknowledged.

Authors' contributions

ZD, LYL designed the topic and the ideas of this research. ZD, LSN, HYJ and YSW prepared and performed the experiments. ZB, ZKK conducted the experiments and analyzed the data. ZYH and HPX ofered help for the analysis of experimental data. ZD, LYL and MGY co-wrote paper. All authors read and approved the fnal manuscript

Funding

This research was supported by the National Natural Science Foundation of China (81772317, 51973060). The funding from the CHUTIAN Scholar Project of Hubei Province and the Key Laboratory for the Synthesis and Application of Organic Functional Molecules, Ministry of Education (2014-KL-004) were also acknowledged.

Ethics approval and consent to participate

All experiment protocols were approved by the Institutional Animal Care and Use Committee (IACUC) of the Animal Experiment Center of Wuhan University of Chinese Medicine (Wuhan, China).

Consent for publication

All authors agree to submission of this work to be published.

Availability of data and materials

All data generated or analysed during this study are included in this published article and its supplementary information files.

Conflicts of interest

The authors declare no competing interests.

References

1. Shi J, Kantoff PW, Wooster R, Farokhzad OC. Cancer nanomedicine: progress, challenges and opportunities. Nat Rev Cancer. 2016;17:20.
2. Bhattarai P, Hameed S, Dai Z. Recent advances in anti-angiogenic nanomedicines for cancer therapy. Nanoscale. 2018,10:5393-5423.
3. Chen Y, Xu Z, Zhu D, Tao X, Gao Y, Zhu H, Mao Z, Ling J. Gold nanoparticles coated with polysarcosine brushes to enhance their colloidal stability and circulation time in vivo. J Colloid Inter. 2016;483:201-210.
4. Jain RK, Stylianopoulos T. Delivering nanomedicine to solid tumors. Nat Rev Clin Oncol. 2010;7:653.
5. Kennedy LC, Bickford LR, Lewinski NA, Coughlin AJ, Hu Y, Day ES, West JL, Drezek RA. A New Era for Cancer Treatment: Gold-Nanoparticle-Mediated Thermal Therapies. Small. 2011;7:169-183.
6. Duan X, Li Y. Physicochemical Characteristics of Nanoparticles Affect Circulation, Biodistribution, Cellular Internalization, and Trafficking. Small. 2013;9:1521-1532.
7. Stylianopoulos T. EPR-effect: utilizing size-dependent nanoparticle delivery to solid tumors. Ther Deliv. 2013;4:421-423.
8. Collette F, Delatouche R, Blanquart C, Gueugnon F, Grégoire M, Bertrand P, Héroguez V. Easy and effective method to produce functionalized particles for cellular uptake. J Polym Sci Part A: Polym Chem. 2013;51:176-189.
9. Salatin S, Maleki Dizaj S, Yari Khosroushahi A. Effect of the surface modification, size, and shape on cellular uptake of nanoparticles. Cell Biol Int. 2015;39:881-890.
10. Meng F, Cheng R, Deng C, Zhong Z. Intracellular drug release nanosystems. Mater Today. 2012;15:436-442.
11. Yang H, Wang Q, Huang S, Xiao A, Li F, Gan L, Yang X. Smart pH/Redox Dual-Responsive Nanogels for On-Demand Intracellular Anticancer Drug Release. ACS Appl Mater Inter. 2016;8:7729-7738.
12. Xu X, Ho W, Zhang X, Bertrand N, Farokhzad O. Cancer nanomedicine: from targeted delivery to combination therapy. Trends Mol Med. 2015;21:223-232.

13. Phapal SM, Sunthar P. Influence of micro-mixing on the size of liposomes self-assembled from miscible liquid phases. Chem Phys Lipids. 2013;172-173:20-30.
14. Chauhan VP, Stylianopoulos T, Martin JD, Popović Z, Chen O, Kamoun WS, Bawendi MG, Fukumura D, Jain RK. Normalization of tumour blood vessels improves the delivery of nanomedicines in a size-dependent manner. Nat Nanotechnol. 2012;7:383.
15. Freiberg S, Zhu XX. Polymer microspheres for controlled drug release. Int J Pharm. 2004;282:1-18.
16. Bar-Zeev M, Livney YD, Assaraf YG. Targeted nanomedicine for cancer therapeutics: Towards precision medicine overcoming drug resistance. Drug Resist Update. 2017;31:15-30.
17. Liao R, Lv P, Wang Q, Zheng J, Feng B, Yang B. Cyclodextrin-based biological stimuli-responsive carriers for smart and precision medicine. Biomater Sci. 2017;5:1736-1745.
18. Albanese A, Tang PS, Chan WCW. The Effect of Nanoparticle Size, Shape, and Surface Chemistry on Biological Systems. Annu Rev Biomed Eng. 2012;14:1-16.
19. Chithrani BD, Ghazani AA, Chan WCW. Determining the Size and Shape Dependence of Gold Nanoparticle Uptake into Mammalian Cells. Nano Lett. 2006;6:662-668.
20. Mock JJ, Barbic M, Smith DR, Schultz DA, Schultz S. Shape effects in plasmon resonance of individual colloidal silver nanoparticles. J Chem Phys. 2002;116:6755-6759.
21. Yallapu MM, Jaggi M, Chauhan SC. Design and engineering of nanogels for cancer treatment. Drug Discov Today. 2011;16:457-463.
22. Beningo KA, Wang Y-l. Fc-receptor-mediated phagocytosis is regulated by mechanical properties of the target. J Cell Sci. 2002;115:849-856.
23. Choi WI, Lee JH, Kim J-Y, Kim J-C, Kim YH, Tae G. Efficient skin permeation of soluble proteins via flexible and functional nano-carrier. J Control Release. 2012;157:272-278.
24. Hasegawa U, Nomura S-iM, Kaul SC, Hirano T, Akiyoshi K. Nanogel-quantum dot hybrid nanoparticles for live cell imaging. Biochem Bioph Res Co. 2005;331:917-921.
25. Ahmad Z, Pandey R, Sharma S, Khuller GK. Pharmacokinetic and pharmacodynamic behaviour of antitubercular drugs encapsulated in alginate nanoparticles at two doses. Int J Antimicrob Ag. 2006;27:409-416.
26. Sahiner N, Godbey WT, McPherson GL, John VT; Microgel, nanogel and hydrogel–hydrogel semi-IPN composites for biomedical applications: synthesis and characterization. Colloid Polym Sci. 2006;284:1121-1129.
27. Choi J-W, Jung S-J, Kasala D, Hwang JK, Hu J, Bae YH, Yun C-O. pH-sensitive oncolytic adenovirus hybrid targeting acidic tumor microenvironment and angiogenesis. J Control Release. 2015;205:134-143.
28. Liu J, Luo Z, Zhang J, Luo T, Zhou J, Zhao X, Cai K. Hollow mesoporous silica nanoparticles facilitated drug delivery via cascade pH stimuli in tumor microenvironment for tumor therapy. Biomaterials. 2016;83:51-65.

29. Mo R, Gu Z. Tumor microenvironment and intracellular signal-activated nanomaterials for anticancer drug delivery. Mater Today. 2016;19:274-283.
30. Ruan S, Yuan M, Zhang L, Hu G, Chen J, Cun X, Zhang Q, Yang Y, He Q, Gao H. Tumor microenvironment sensitive doxorubicin delivery and release to glioma using angiopep-2 decorated gold nanoparticles. Biomaterials. 2015;37:425-435.
31. Meyer AJ, Brach T, Marty L, Kreye S, Rouhier N, Jacquot J-P, Hell R. Redox-sensitive GFP in Arabidopsis thaliana is a quantitative biosensor for the redox potential of the cellular glutathione redox buffer. Plant J. 2007;52:973-986.
32. Tu Y, Peng F, White PB, Wilson DA. Redox-Sensitive Stomatocyte Nanomotors: Destruction and Drug Release in the Presence of Glutathione. Angew Chem Int Ed. 2017;56:7620-7624.
33. Ralph P, Moore MA, Nilsson K. Lysozyme synthesis by established human and murine histiocytic lymphoma cell lines. J Exp Med. 1976;143:1528-1533.
34. Serra C, Vizoso F, Alonso L, Rodríguez JC, González LO, Fernández M, Lamelas ML, Sánchez LM, García-Muñiz JL, Baltasar A, Medrano J. Expression and prognostic significance of lysozyme in male breast cancer. Breast Cancer Res. 2002;4:R16.
35. Younes I, Rinaudo M. Chitin and Chitosan Preparation from Marine Sources. Structure, Properties and Applications. Mar Drugs. 2015;13:1133-1174..
36. Zou P, Yang X, Wang J, Li Y, Yu H, Zhang Y, Liu G. Advances in characterisation and biological activities of chitosan and chitosan oligosaccharides. Food Chem. 2016;190:1174-1181.
37. Ju C, Mo R, Xue J, Zhang L, Zhao Z, Xue L, Ping Q, Zhang C. Sequential Intra-Intercellular Nanoparticle Delivery System for Deep Tumor Penetration. Angew Chem Int Ed. 2014;53:6253-6258.
38. Sun Q, Ojha T, Kiessling F, Lammers T, Shi Y. Enhancing Tumor Penetration of Nanomedicines. Biomacromolecules. 2017;18:1449-1459.
39. Zhong Y, Meng F, Deng C, Zhong Z. Ligand-Directed Active Tumor-Targeting Polymeric Nanoparticles for Cancer Chemotherapy. Biomacromolecules. 2014;15:1955-1969.
40. 40. Moeini A, Cimmino A, Dal Poggetto G, Di Biase M, Evidente A, Masi M, Lavermicocca P, Valerio F, Leone A, Santagata G, Malinconico M. Effect of pH and TPP concentration on chemico-physical properties, release kinetics and antifungal activity of Chitosan-TPP-Ungeremine microbeads. Carbohyd Polym. 2018;195:631-641.
41. 41. Baran T, Menteş A, Arslan H. Synthesis and characterization of water soluble O-carboxymethyl chitosan Schiff bases and Cu(II) complexes. Int J Biol Macromol. 2015;72:94-103.
42. 42. Kaya M, Cakmak YS, Baran T, Asan-Ozusaglam M, Mentes A, Tozak KO. New chitin, chitosan, and O-carboxymethyl chitosan sources from resting eggs of Daphnia longispina (Crustacea); with physicochemical characterization, and antimicrobial and antioxidant activities. Biotechnol Bioproc E. 2014;19:58-69.
43. 43. Niu G, Yang Y, Zhang H, Yang J, Song L, Kashima M, Yang Z, Cao H, Zheng Y, Zhu S, Yang H. Synthesis and characterization of acrylamide/N-vinylpyrrolidone copolymer with pendent thiol groups for ophthalmic applications. Acta Biomater. 2009;5:1056-1063.

44. 44. Gao X, Zhou Y, Ma G, Shi S, Yang D, Lu F, Nie J. A water-soluble photocrosslinkable chitosan derivative prepared by Michael-addition reaction as a precursor for injectable hydrogel. Carbohyd Polym. 2010;79:507-512.
45. 45. Kumar S, Garg P, Pandey S, Kumari M, Hoon S, Jang K-J, Kapavarapu R, Choung P-H, Sobral AJFN, Hoon Chung J. Enhanced chitosan–DNA interaction by 2-acrylamido-2-methylpropane coupling for an efficient transfection in cancer cells. J Mater Chem B. 2015;3:3465-3475.
46. 46. Kedmi R, Ben-Arie N, Peer D. The systemic toxicity of positively charged lipid nanoparticles and the role of Toll-like receptor 4 in immune activation. Biomaterials. 2010;31:6867-6875.
47. 47. Han K, Zhang W-Y, Zhang J, Lei Q, Wang S-B, Liu J-W, Zhang X-Z, Han H-Y. Acidity-Triggered Tumor-Targeted Chimeric Peptide for Enhanced Intra-Nuclear Photodynamic Therapy. Adv Funct Mater. 2016;26:4351-4361.
48. 48. Fan H, Yan G, Zhao Z, Hu X, Zhang W, Liu H, Fu X, Fu T, Zhang X-B, Tan W. A Smart Photosensitizer–Manganese Dioxide Nanosystem for Enhanced Photodynamic Therapy by Reducing Glutathione Levels in Cancer Cells. Angew Chem Int Ed. 2016;55:5477-5482.
49. 49. Cheng R, Feng F, Meng F, Deng C, Feijen J, Zhong Z. Glutathione-responsive nano-vehicles as a promising platform for targeted intracellular drug and gene delivery. J Control Release. 2011;152:2-12.
50. 50. Quesada M, Muniesa C, Botella P. Hybrid PLGA-Organosilica Nanoparticles with Redox-Sensitive Molecular Gates. Chem Mater. 2013;25:2597-2602.
51. 51. Vicent MJ, Greco F, Nicholson RI, Paul A, Griffiths PC, Duncan R. Polymer Therapeutics Designed for a Combination Therapy of Hormone-Dependent Cancer. Angew Chem Int Ed. 2005;44:4061-4066.
52. 52. Meng H, Xue M, Xia T, Zhao Y-L, Tamanoi F, Stoddart JF, Zink JI, Nel AE. Autonomous in Vitro Anticancer Drug Release from Mesoporous Silica Nanoparticles by pH-Sensitive Nanovalves. J Am Chem Soc. 2010;132:12690-12697.
53. 53. Hajji S, Khedir SB, Hamza-Mnif I, Hamdi M, Jedidi I, Kallel R, Boufi S, Nasri M. Biomedical potential of chitosan-silver nanoparticles with special reference to antioxidant, antibacterial, hemolytic and in vivo cutaneous wound healing effects. BBA Gen Subjects. 2019;1863:241-254.
54. 54. Rampino A, Borgogna M, Blasi P, Bellich B, Cesàro A. Chitosan nanoparticles: Preparation, size evolution and stability. Int J Pharm. 2013;455:219-228.
55. 55. Sun X, Tang Z, Pan M, Wang Z, Yang H, Liu H. Chitosan/kaolin composite porous microspheres with high hemostatic efficacy. Carbohyd Polym. 2017;177:135-143.
56. 56. Zhu A, Yuan L, Liao T. Suspension of Fe3O4 nanoparticles stabilized by chitosan and o-carboxymethylchitosan. Int J Pharm. 2008;350:361-368.
57. 57. Rieger J, Kellermeier M, Nicoleau L. Formation of Nanoparticles and Nanostructures—An Industrial Perspective on CaCO3, Cement, and Polymers. Angew Chem Int Ed. 2014;53:12380-12396.
58. 58. Mohtaram NK, Montgomery A, Willerth SM. Biomaterial-based drug delivery systems for the controlled release of neurotrophic factors. Biomed Mater. 2013;8:

59. 59. Raemdonck K, Demeester J, De Smedt S. Advanced nanogel engineering for drug delivery. Soft Matter. 2009;5:707-715.
60. 60. Maggini L, Cabrera I, Ruiz-Carretero A, Prasetyanto EA, Robinet E, De Cola L. Breakable mesoporous silica nanoparticles for targeted drug delivery. Nanoscale. 2016;8:7240-7247.
61. 61. Zhang L, Guo R, Yang M, Jiang X, Liu B. Thermo and pH Dual-Responsive Nanoparticles for Anti-Cancer Drug Delivery. Adv Mater. 2007;19:2988-2992.
62. 62. Adeyemi OS, Sulaiman FA. Evaluation of metal nanoparticles for drug delivery systems. J Biomed Res. 2015;29:145-149.
63. 63. Yi J-M, Huan X-J, Song S-S, Zhou H, Wang Y-Q, Miao Z-H. Triptolide Induces Cell Killing in Multidrug-Resistant Tumor Cells via CDK7/RPB1 Rather than XPB or p44. Mol Cancer Ther. 2016;15:
64. 64. Agudelo D, Bourassa P, Bérubé G, Tajmir-Riahi H-A. Intercalation of antitumor drug doxorubicin and its analogue by DNA duplex: Structural features and biological implications. Int J Biol Macromol. 2014;66:144-150.
65. 65. Huang P, Chen Y, Lin H, Yu L, Zhang L, Wang L, Zhu Y, Shi J. Molecularly organic/inorganic hybrid hollow mesoporous organosilica nanocapsules with tumor-specific biodegradability and enhanced chemotherapeutic functionality. Biomaterials. 2017;125:23-37.
66. 66. Sun L, Liu T, Li H, Yang L, Meng L, Lu Q, Long J. Fluorescent and Cross-linked Organic–Inorganic Hybrid Nanoshells for Monitoring Drug Delivery. ACS Appl Mater Inter. 2015;7:4990-4997.
67. 67. Wang J, Wang L, Zhou Z, Lai H, Xu P, Liao L, Wei J. Biodegradable Polymer Membranes Applied in Guided Bone/Tissue Regeneration: A Review. Polymers. 2016;8:115.
68. 68. Ehlerding EB, Chen F, Cai W. Biodegradable and Renal Clearable Inorganic Nanoparticles. Adv Sci. 2016;3:
69. 69. Janes KA, Fresneau MP, Marazuela A, Fabra A, Alonso MaJ. Chitosan nanoparticles as delivery systems for doxorubicin. J Control Release. 2001;73:255-267.
70. 70. He Q, Shi J. MSN Anti-Cancer Nanomedicines: Chemotherapy Enhancement, Overcoming of Drug Resistance, and Metastasis Inhibition. Adv Mater. 2014;26:391-411.
71. 71. Peng X, Wu T, Fan J, Wang J, Zhang S, Song F, Sun S. An Effective Minor Groove Binder as a Red Fluorescent Marker for Live-Cell DNA Imaging and Quantification. Angew Chem Int Ed. 2011;50:4180-4183.
72. 72. Lin Y-S, Haynes CL. Impacts of Mesoporous Silica Nanoparticle Size, Pore Ordering, and Pore Integrity on Hemolytic Activity. J Am Chem Soc. 2010;132:4834-4842.

Table

Table 1. Hydrodynamic Size, Zeta potential, and drug-loading capacity of nanogels.

Sample	Size (nm)	Zeta (mV)	EE (%)[a]	LC (%)[b]
CTCB	190.6 ± 5.3	39.2 ± 7.1	-	-
CTCP	95.8 ± 1.5	-28.1 ± 2.1	-	-
DOX@CTCB	327.3 ± 5.1	20.1 ± 4.8	13.4 ± 6.2	1.1 ± 0.5
DOX@CTCP	128.7 ± 2.4	-26.4 ± 1.1	92.1 ± 3.6	5.9 ± 0.3

[a] Encapsulation Efficiency (EE) = 100 * W_t/W_0, W_0 is the drug for loading, and W_t is the packaged drug. [b] Loading Capacity (LC) = 100 * W_t/W, W_t represents the drugs that have been loaded into the nanogels, and W is the total weight of the nanogels.

Figures

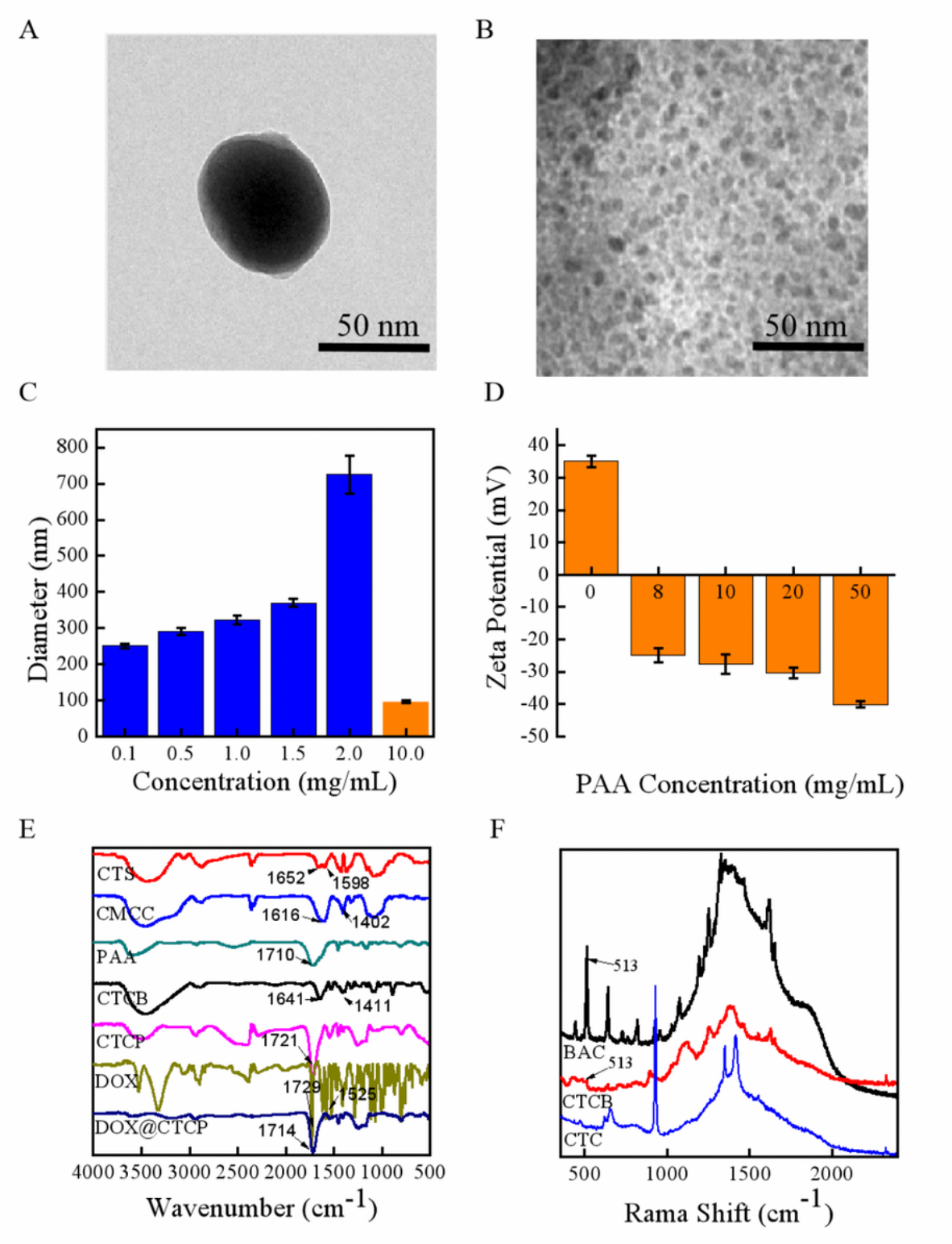

Figure 1

Preparation and characterization of biodegradable nanogels. TEM images of CTCP nanogels (A) before and (B) after treatment with 10 mM DTT for 1 h (Scale bar = 50 nm). (C) Change of hydrodynamic sizes of CTCB nanogels as a function of TPP concentrations (blue bars), and of the optimal CTCP nanogels after conjugation with PAA (yellow bar). (D) Variation of biodegradable nanogels in Zeta potentials before and after PAA decoration at different concentrations. (E) Fourier-transform infrared (FTIR) spectra of CTS,

CMCC, PAA, CTCB, CTCP, DOX, DOX@CTCP. (F) Rama spectra of the nanogels before and after crosslinking with BAC.

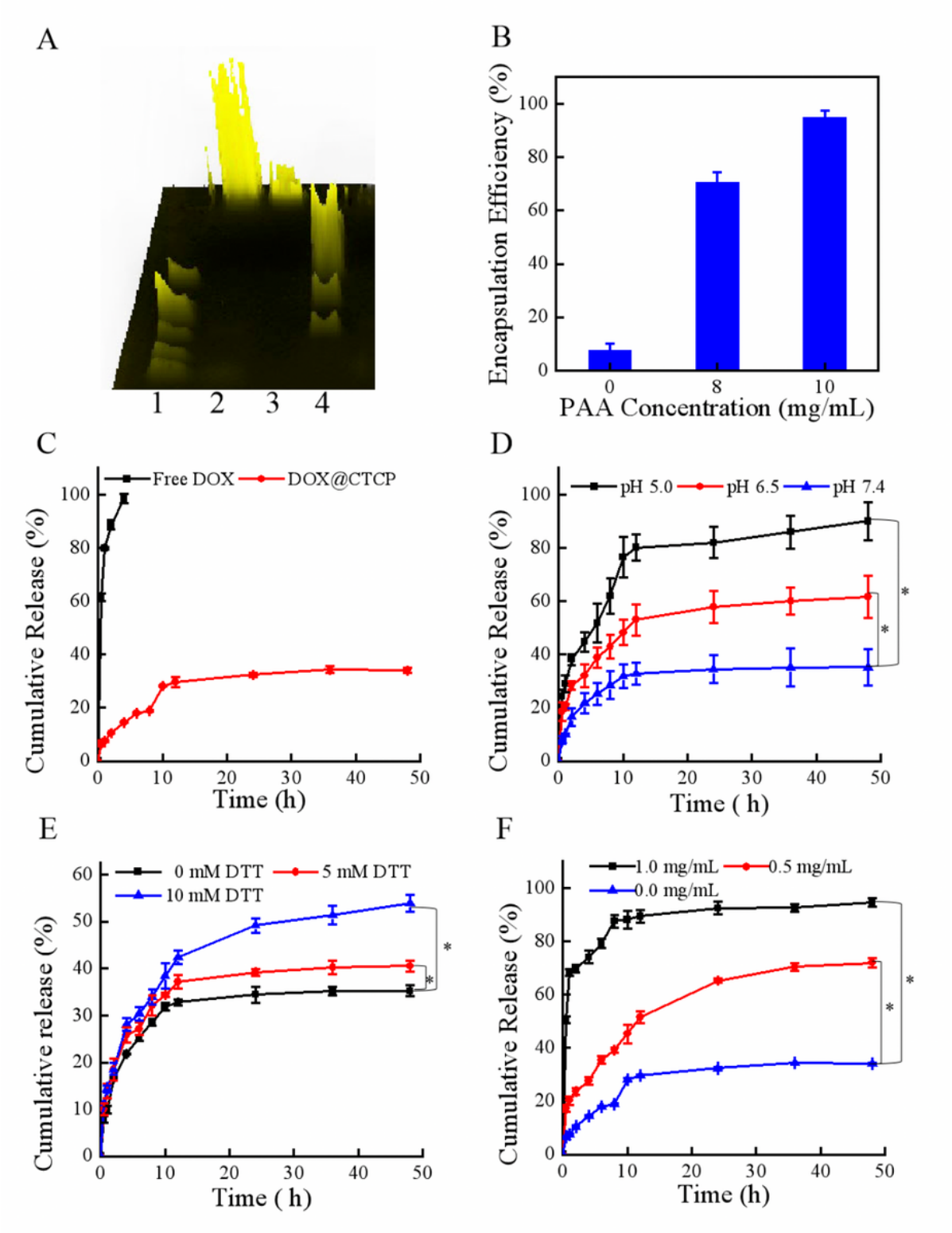

Figure 2

Drug loading selectivity of the nanogels as well as their tumor-stimulated drug release properties. (A) 3D Agarose gel electrophoresis of plasmid DNA before and after encapsulation into CTCB nanogels (Lane 1: Marker D2000 indicating the DNA before construction; Lane 2: 5 μL precipitate of plasmid DNA-loaded

CTCB nanogels being centrifugated; Lane 3: 5 µL supernatant of plasmid DNA-loaded CTCB nanogels after centrifugation; Lane 4: Marker IV indicating red fluorescent plasmid DNA after construction). (B) Drug encapsulation efficiency of the nanogels before and after conjugation with PAA at different concentrations (0 mg/mL - 1.0 mg/mL). In vitro DOX release profile of (C) free DOX and DOX@CTCP in PBS buffer at pH 7.4 and 37 °C; DOX release from DOX@CTCP in PBS (D) at 7.4, 6.5 and 5.0 pH values, (E) in different concentrations of DTT (5.0 mM and 10.0 mM), and (F) in the presence of different concentrations of lysozyme (0 mg/mL - 1.0 mg/mL) (± standard deviation, n = 3, *P < 0.05).

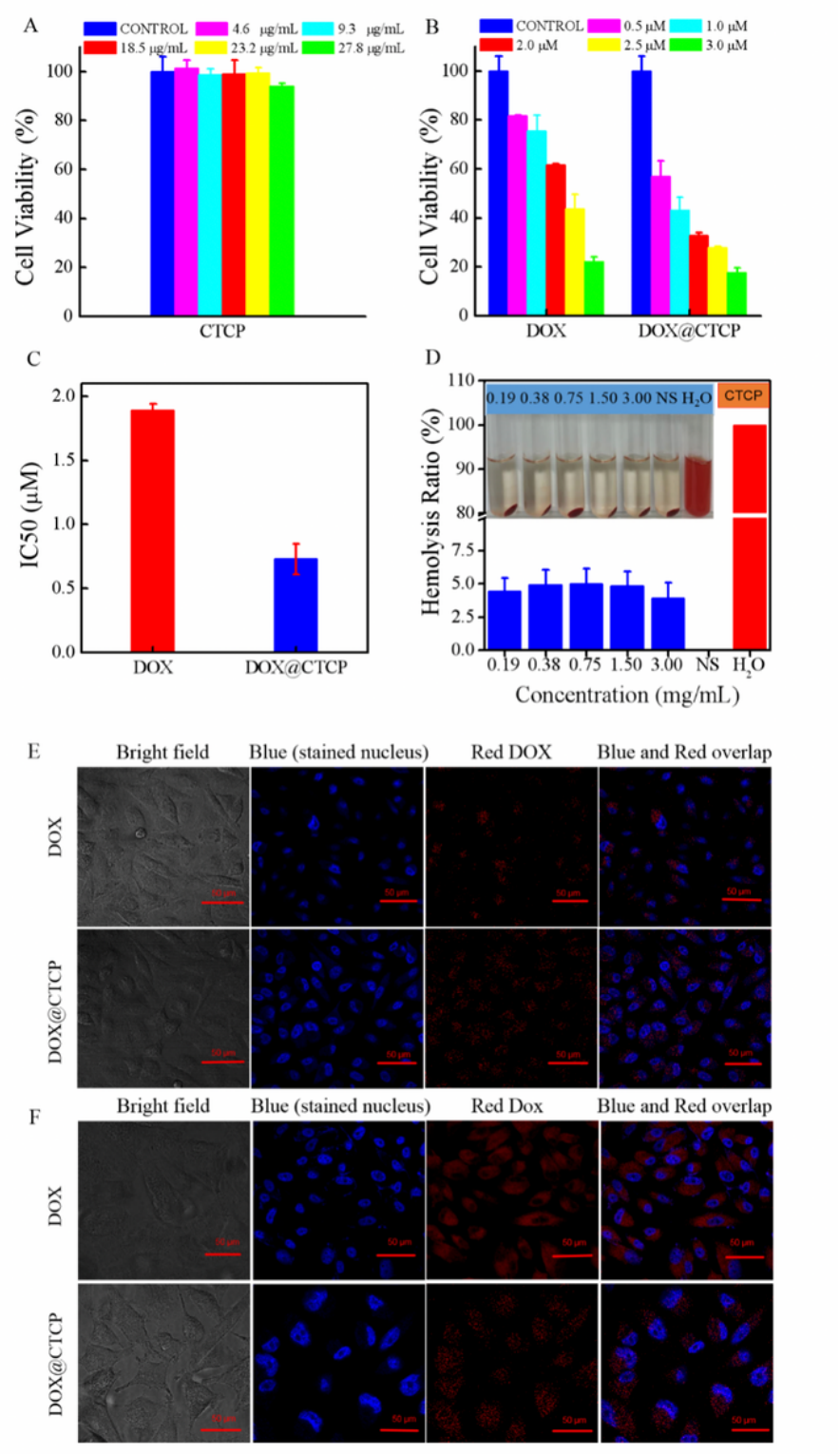

Figure 3

In vitro biocompatibility and toxicity. (A) A549 cell viability exposed to CTCP nanogels at different concentrations for 48 h. (B) A549 cell viability exposed to free DOX and DOX@CTCP (at an equivalent DOX concentration) for 48 h. (C) IC50 of A549 cells exposed to free DOX and DOX@CTCP (at an equivalent DOX concentration) for 48 h. (D) Hemolysis assay of Red Blood Cell (RBC) incubated with CTCP nanogels at different concentrations (NS: normal saline, 0.9% saline injection solution, negative control; H2O: sterile purified water, positive control). Fluorescence microscopy images of A549 cells after incubation with free DOX or DOX@CTCP (2 μM DOX) for (E) 4 h and (F) 24 h, respectively.

Figure 4

In vivo antitumor activity of DOX@CTCP hepatocarcinoma tumor-bearing mice. (A) Relative tumor volume in tumor-bearing C75BL/6J male mice. (B) Percentage of the mice that survived over the indicated time. (C) Body weight of the tumor-bearing mice. (D) Representative images of resected tumors after 15 d of DOX@CTCP treatment and after 7 d of free DOX treatment. H&E staining of (E) tumor and (F) vital organ (heart, liver, spleen, and kidney) sections; scale bar: 200 μm.

Supplementary Files

This is a list of supplementary files associated with this preprint. Click to download.

- SupplementaryMaterial.doc